Title

Insight on the antibacterial mechanism of Cu-enriched sol-gel coatings employing proteomics

Authors

Francisco Romero-Gavilán[1*&], Iñaki García-Arnáez[2&], Andreia Cerqueira[1], Loredana Scalschi[3], Begonya Vicedo[3], Alejandro Villagrasa[1], Raúl Izquierdo[1], Mikel Azkargorta[4], Félix Elortza[4], Mariló Gurruchaga[2], Isabel Goñi[2], Julio Suay[1]

[1]Department of Industrial Systems Engineering and Design, Universitat Jaume I, Av. Vicent Sos Baynat s/n, 12071 Castellón de la Plana, Spain

[2]Departament of Polymers and Advanced Materials: Physics, Chemistry and Technology, Universidad del País Vasco, P. M. de Lardizábal, 3, 20018 San Sebastián, Spain

[3]Department of Biology, Biochemistry and Natural Sciences, Universitat Jaume I, Av. Vicent Sos Baynat s/n, 12071 Castellón de la Plana, Spain

[4]Proteomics Platform, CIC bioGUNE, Basque Research and Technology Alliance (BRTA), CIBERehd, ProteoRed-ISCIII, Bizkaia Science and Technology Park, 48160 Derio, Spain

[&] Equal contribution

* Corresponding autor: Francisco Romero-Gavilán

Departamento de Ingeniería de Sistemas Industriales y Diseño

Avda. Vicent Sos Baynat s/n, Campus del Ríu Sec

12071 – Castelló de la Plana (España)

E-mail: gavilan@uji.es

Abstract

Advanced antibacterial biomaterials can help reduce the severe consequences of infections. Using copper compounds is an excellent option to achieve this goal; they offer a combination of regenerative and antimicrobial functions. In this study, new $CuCl_2$-doped sol-gel coatings were developed and physicochemically characterised. Their osteogenic and inflammatory responses were tested *in vitro* using human osteoblasts and THP-1 macrophages. Their antibacterial effect was evaluated using *Escherichia coli* and *Staphylococcus aureus*. The Cu influence on the adsorption of human serum proteins was analysed employing proteomics. The materials released Cu^{2+} and were not cytotoxic. The osteoblasts in contact with these materials showed an increased ALP, BMP2 and OCN gene expression. The THP-1 showed an increase in pro-inflammatory markers related to M1 polarization. Moreover, Cu-doped coatings displayed a potent antibacterial behaviour against *E. coli* and *S. aureus*. The copper ions affected the adsorption of proteins related to immunity, coagulation, angiogenesis, fibrinolysis, and osteogenesis. Interestingly, the coatings had increased affinity to proteins with antibacterial functions and proteins linked to the complement system activation that can lead to a direct bacterial killing via large pore-forming complexes. These results contribute to our understanding of the antibacterial mechanisms of Cu-biomaterials and their interaction with biological systems.

Keywords:

Biomaterials; dental implants; alkoxysilanes; copper; peri-implantitis

1. Introduction

Copper (Cu) is an essential micronutrient involved in diverse metabolic processes, known for promoting osteogenesis and angiogenesis [1], while improving the antimicrobial properties of biomaterials [2]. Yang *et al.* [3] have found that Cu-doped Ti6AL4V alloy has a significant antibacterial effect both *in vitro* and *in vivo* (implanted into an infected bone defect). Cu ions released from glass nanopowders cause a significant reduction in the growth rate of *Bacillus cereus*, *Staphylococcus aureus* and *Pseudomonas aeruginosa* bacteria [4]. Moreover, the nanocrystalline Ti-Cu alloys show antibacterial activity against *Escherichia coli* and *S. aureus*, maintaining their biocompatible character with osteoblastic cells [5]. The strong antibacterial potential of this element and its low cytotoxicity make copper, either in cation or in metal form, a promising dopant for biomaterials. The Cu ions can promote the proliferation and osteogenic differentiation of mesenchymal stem cells [6]. Huang *et al.* [7] have examined the effects of adding Cu to a bioceramic coating obtained by micro-arc oxidation and hydrothermal treatment. They have found that the release of Cu^{2+} enhances gene expression of SaOS-2 osteoblast alkaline phosphatase (ALP), collagen I and osteocalcin (BGLAP). Substituting the Ca^{2+} ions with Cu^{2+} in a hydroxyapatite coating for Ti implants promotes adhesion, proliferation, collagen secretion, ALP activity and mineralisation in neonatal rat calvaria bone osteoblasts [8]. Cu can also stimulate angiogenesis, process essential for bone regeneration. It has been reported that Cu^{2+} extracted from a bioactive glass scaffold strongly increases the secretion of vascular endothelial growth factor (VEGF) in human dermal microvascular endothelial cells (HDMEC) in co-culture with bone marrow-derived mesenchymal stem cells [9]. Romero-Sanchez *et al.* [10] have tested the biological effects of ions produced by a Cu-doped mesoporous bioactive glass on bovine aorta endothelial cells (BAEC) and in zebrafish embryos *in vivo*. They have shown an increased endothelial cell viability and an enhancement in vessels formation *in vivo*.

Sol-gel coatings represent an interesting approach to modifying metallic surfaces, such as titanium (Ti), to improve their use in biomedical applications [11]. The sol-gel networks can also be employed as release vehicles for therapeutic substances; the osteogenic and antibacterial agents can be entrapped and then released in a controlled manner [12]. Hybrid sol-gel materials based on methyltrimethoxysilane (MTMOS) and tetraethyl orthosilicate (TEOS) precursors have been already developed, and their successful application as coatings has been described [13–15]. A material based on 70% MTMOS and 30% TEOS has shown strong potential as a bioactivate coating for sandblasted, acid-etched Ti implants [15]. Thus, this material is a good candidate for a Cu delivery vehicle in Ti prostheses.

As soon as an implant is put in contact with living tissues, the first phenomenon that takes place is the adsorption of proteins on its surface [16]. The composition and conformation of the protein layer formed on the material can affect the different biological responses activated after implantation and determine the success of the surgery [17]. Proteomics offers powerful tools for analysing complex

mixtures of proteins, such as the protein layers formed on biomaterials [18]. Cerqueira *et al.* [19] have studied the protein layers adsorbed onto magnesium-enriched surfaces. Many proteins associated with cell adhesion were found on these surfaces, explaining the improved osteoblast adhesion to these Mg-enriched materials. The kinetics of protein adsorption to a Ca-biomimetic treatment applied onto Ti has also been studied using mass spectrometry. Adsorption/desorption patterns of key proteins associated with the coagulation system and the immune response could explain the differences between *in-vitro* blood clotting and inflammatory potential of the Ti and the Ca-modified implants [20]. Examining the Cu effects on the protein adsorption onto biomaterials should improve our understanding of the role of this element in tissue regeneration and its ability to prevent bacterial infections.

Here, we present the first MS-proteomic study focusing on the protein adsorption onto biomaterials with antibacterial behaviour. We developed new antibacterial sol-gel coatings with different $CuCl_2$ amounts (0.1, 0.5, 1 and 3 wt%). The obtained coatings were characterised physicochemically, and their osteogenic, inflammatory, and antibacterial potentials were assessed *in vitro*. Profiling how protein adsorption patterns on the coatings are affected by increasing Cu^{2+} doping and their correlation with the *in vitro* biological response can provide new insights into the action mechanism of these Cu-enriched treatments.

2. Experimental

2.1. Sol-gel synthesis and sample preparation

The Cu-enriched coatings were obtained using the sol-gel synthesis route. MTMOS and TEOS precursors, in the optimal molar ratio of 7:3 [15], were mixed with 2-propanol (50 vol%). The monomers were hydrolysed by adding the corresponding stoichiometric amount of acidified water (0.1M HNO_3) at 1 drop s^{-1}. The $CuCl_2$ was incorporated into this solution before adding it to the precursors. The sol-gel mixtures were kept under stirring for 1 h and then left to rest for 1 h. The materials with 0.1, 0.5, 1 and 3 wt% $CuCl_2$ are referred to as 0.1Cu, 0.5Cu, 1Cu and 3Cu, respectively. The wt% content is relative to the total amount of precursors. The sol-gel composition without Cu (0Cu) was used as a control. All the reagents were purchased from Merck (Darmstadt, Germany). Grade-4 Ti discs (Ilerimplant-GMI SL., Lleida, Spain), sandblasted and acid-etched (SAE), were employed as substrates. The SAE preparation is described in the study of Romero-Gavilán *et al.* [21]. Depending on the experiment, the discs of 1-mm thickness and different diameters (12 and 10 mm) were used. The sol-gel material was applied onto the discs using a dip-coater (KSV DC; KSV NIMA, Espoo, Finland). They were immersed in the mixture at 60 cm min^{-1}, kept immersed for 1 min and then removed at 100 cm min^{-1}. For the hydrolytic degradation and Cu-ion release measurements, the coatings were prepared on glass slides cleaned with HNO_3 solution (25% v/v) in an ultrasonic bath (Sonoplus HD 3200) for 20 min and then washed

with distilled water under the same conditions. The sol-gel was applied by casting, using the same amount of material in all cases. To study the chemistry of the materials, free films were obtained by pouring 5 mL of sol-gel preparation into a non-stick Teflon mould. Finally, the samples were cured for 2 h at 80 °C in all cases.

2.2. Physicochemical characterisation

The morphology of the coatings applied on 12-mm Ti discs was studied using a Leica-Zeiss LEOS scanning electron microscope (SEM; Leica, Wetzlar, Germany) coupled to an Oxford INCA 250 energy dispersive X-ray spectrometer (EDX; Oxford Instruments, Abingdon, UK). The samples were sputtered with Pt before SEM examinations to improve their conductivity. The sample roughness was determined using an optical profilometer (interferometric and confocal) PLm2300 (Sensofar, Barcelona, Spain). Three different 12-mm coated samples were analysed for each condition (three measurements for each sample). The results were expressed as the Ra parameter (arithmetic average roughness). A Thermo Nicolet 6700 Fourier-transform infrared spectrometer (FTIR; Thermo Fisher Scientific, Waltham, MA, USA) with an attenuated total reflection system (ATR) was used to analyse the chemistry of the obtained materials. The spectra were measured in the 400 to 4000 cm^{-1} range. For the structural analysis, a Bruker D4-Endeavor diffractometer (XRD; Bruker, Billerica, MA, USA) was employed. The spectra were recorded in the range of 5–70° (2θ) with an operating voltage of 40 kV, the filament current of 40 mA, step size of 0.05°(2θ) and the scanning rate of 4 s $step^{-1}$, with filtered CuKα radiation (λ = 1.54 A). A Bruker 400 Avance III WB Plus solid-state nuclear magnetic resonance spectrometer (^{29}Si-NMR; Bruker) coupled with a cross-polarisation magic-angle spinning (CP-MAS) probe for solid samples was used to analyse the crosslinking degree of obtained materials. The spinning speed was 7.0 kHz, and the Bruker standard pulse sequence of 79.5-MHz frequency, 55-kHz spectral width, 2-ms contact time and 5-s delay time were used. The hydrolytic degradation kinetics of the coating was measured by incubating the coated glass slides in 50 mL of distilled water at 37 °C for 7, 14, 28, 49 and 63 days. The degradation of the coatings was expressed as the percentage of mass lost. Three replicates were analysed for each condition. The release of Cu^{2+} ions from the coatings was obtained using an inductively coupled plasma atomic emission spectrometer (ICP-AES; Activa, Horiba Jobin Yvon IBH Ltd., Glasgow, UK). Coatings applied on glass slides were incubated in ddH_2O at 37 °C, and 0.5-mL aliquots were taken after 2, 4, 8, 24, 72, 168, 336, 504 and 672 h. The experiment was performed in triplicate.

2.3. *In vitro* experimentation

2.3.1 Cell culture

Human osteoblasts (HOb) and human monocyte (THP-1) cells were cultured in Dulbecco's Modified Eagle Medium (DMEM; Merck) and RPMI-1640 Medium (Merck), respectively. In both cases, the medium was supplemented with 10% FBS (Gibco, Thermo Fisher Scientific) and 1%

penicillin/streptomycin (Biowest, Riverside, MO, USA). Cell incubation was carried out at 37 °C in a humidified atmosphere with 5% CO_2. In the case of HOb, the medium was replaced after 24 h with osteogenic medium composed of low-glucose DMEM, 1% penicillin/streptomycin, 10% FBS, 1% ascorbic acid (5 mg mL^{-1}) and 0.21% β-glycerol phosphate. The THP-1 cells were induced to differentiate to macrophages using phorbol 12-myristate 13-acetate (PMA; Merck). The culture medium was changed every two days. Coatings applied on 10-mm Ti discs were employed in *in vitro* testing and cultures without biomaterials were used as controls.

2.3.2. Cytotoxicity

Material cytotoxicity tests were carried out according to the ISO 10993-5:2009 Annex I norm. Briefly, the HOb cells were seeded at a density of 1 x 10^4 cell cm^{-2} on 96-well plates (Corning Inc.; Somerville, MA, USA) for 24 h. Biomaterials were also incubated for 24 h with the same medium in 48-well plates (Corning Inc.). After incubation, the cell culture medium from 96-well plate was replaced by the medium exposed to the materials. To assess cell viability, CellTiter 96® Proliferation Assay (MTS; Promega, Madison, WI, USA) was performed according to manufacturer's guidelines. Cells incubated with latex (cytotoxic agent) were employed as a positive control, while the cultures without biomaterials were used as a negative control. A biomaterial was considered cytotoxic when the cell viability fell below 70%.

2.3.3. Cell proliferation

Cell proliferation was analysed using CellTiter 96® Proliferation Assay (MTS, Promega). The HOb cells were seeded in 48-well plates at the density of 7.5 x 10^3 cells cm^{-2} and proliferation was evaluated following the manufacturer's instructions after 1, 3 and 7 days. Absorbance was measured at 490 nm in a Multiskan FC microplate reader (Thermo Fisher Scientific).

2.3.4. ALP activity and ARS mineralisation

The alkaline phosphatase (ALP) activity was measured employing the conversion of p-nitrophenylphosphate (p-NPP) to p-nitrophenol. The HOb cells were seeded on the different surfaces in 48-well plates at the density of 2.5 x 10^4 cells cm^{-2} for 7 and 14 days. ALP activity was measured following the protocol described in Cerqueira *et al.* [22]. Total protein content was obtained using the Pierce BCA assay kit (Thermo Fisher Scientific) and used to normalise the ALP levels. To assess the mineralisation ability of HOb, the cells were cultured for 7 and 14 days in 48-well plates at the initial density of 2.5 x 10^4 cells cm^{-2}. The calcium deposits were stained with Alizarin Red S (ARS). The ARS was extracted with cetylpyridinium chloride in 10 mM Na_2HPO_4 (pH 7) and quantified at 540 nm. The three reagents were purchased from Merck.

2.3.5. Quantitative real-time PCR

To study gene expression of inflammatory and osteogenic targets, the THP-1 and HOb cells were cultured with the biomaterials, and RNA was isolated to synthesise cDNA. The THP-1 cells were seeded

in 48-well plates at the density of 1.5 x 10^5 cells cm^{-2} for 24 h and at 3 x 10^5 cells cm^{-2} for 72 h. The HOb cells were seeded at the density of 2.5 x 10^4 cells cm^{-2} in 48-well plates and cultured for 7 and 14 days. Total RNA was extracted using TRIzol method according to the previously published protocol [22], and its concentration was measured using a Nanodrop 2000c spectrophotometer (Thermo Fisher Scientific). For cDNA synthesis, 500 ng of total RNA was turned into cDNA using PrimeScript RT Reagent Kit (Perfect Real Time; TAKARA Bio Inc., Shiga, Japan). The reverse transcription was performed under the following conditions: 37 °C for 15 min, 85 °C for 5 s and a final hold at 4 °C. The expression of target genes was assessed by quantitative real-time PCR (StepOne Plus™ Real-Time PCR System; Applied Biosystems®, Thermo Fisher Scientific). The reactions were carried out in 96-well plates (Thermo Fisher) as previously described [22] and results were normalised to the GAPDH housekeeping gene. The results were analysed using the StepOne Plus™ Software 2.3 (Thermo Fisher Scientific), employing the $2^{-\Delta\Delta}$Ct method, and normalised to the samples from wells without any materials (experimental controls). **Table S1** shows primers designed with PRIMER3plus software from the sequences obtained from NCBI and purchased from Thermo Fisher Scientific.

2.3.6. Cytokine analysis

To examine the secretome of cells cultured with different materials, the THP-1 cells were seeded in 48-well plates at the density of 3 x 10^5 and 1.5 x 10^4 and incubated for 24 h and 72 h, respectively. Then, the culture media were collected and frozen. To study the inflammatory environment affected by Cu, we measured the concentration of two cytokines, tumour necrosis factor α (TNF-α) and transforming growth factor β (TGF- β), using ELISA kits (Invitrogen, Thermo Fisher Scientific) according to the manufacturer's guidelines.

2.4. Protein layer adsorption and proteomic analysis

To obtain the serum protein layer formed on the different surfaces, the coated Ti discs (12-mm diameter) were incubated with 1 mL of human serum from male AB plasma (Merck) for 3 h (37 °C, 5 % CO_2) in 24-well plates (Corning Inc.). Non-adsorbed proteins were removed by rinsing the discs five times with ddH_2O and once with the 50 mM Tris–HCl, pH 7.0, containing 100 mM NaCl. The adsorbed protein layer was eluted with the buffer consisting of 2 M thiourea, 7 M urea, 4% CHAPS and 200 mM dithiothreitol. All the reagents were purchased from Merck. Four independent replicates were analysed for each type of surface; each replicate was made by pooling the protein layer eluates from four discs. Pierce BCA assay kit (Thermo Fisher) was employed to measure the total protein concentration in the serum. The protein analysis was performed using a Evosep ONE (Evosep, Odense C, Denmark) chromatograph coupled to a hybrid trapped ion mobility-quadrupole time of flight mass spectrometer (timsTOF Pro with PASEF; Bruker, Billerica, MA, USA). Each sample was analysed in quadruplicate. Protein identification was carried out using the MaxQuant software (http://maxquant.org/). The differential analysis of the protein layers obtained from the Cu-enriched

coatings and the control 0Cu was performed employing the Perseus platform (https://www.maxquant.org/perseus/). The functional studies were conducted using PANTHER (http://www.pantherdb.org/) and DAVID v6.8 (Database for Annotation, Visualization and Integrated Discovery, https://david.ncifcrf.gov/) software and the UniProt database (https://www.uniprot.org/). The UniProt ID codes were utilised as protein names.

2.5. Antimicrobial activity

Before testing the antimicrobial properties of the materials, the Cu-doped coatings were sterilised under UV light (30 minutes on each side). Two bacterial strains were used, *S. aureus* strain ATCC2913 and *E. coli* strain NCIMB9484. Both strains were obtained from the Spanish Type Culture Collection (CECT) and stored in glycerol at -80 °C. One day before antimicrobial efficacy testing, a small amount of the suspension from a frozen sample was inoculated onto Luria-Bertani agar medium and incubated for 24 h at 37 °C. From the obtained culture, a suspension was prepared in 10 mM $MgSO_4$ and adjusted to a concentration of 10^7 cfu mL^{-1}. The samples of the Cu-doped coatings were placed in sterile 48-well plates. Then, 10-µL aliquots of the bacterial suspension were transferred to 990 µL of Luria-Bertani Broth (LB) medium (previously diluted 1:50), to obtain a final bacteria concentration of 10^5 cfu mL^{-1}, and added to each well. The plates were shaken at 90 rpm (at 37 °C for 24 h). After 24 h of exposure to the Cu-doped coatings, 1000-µL suspension aliquots were collected and four serial decimal dilutions were prepared. Five µL of each dilution was inoculated on a solid LB plate. After 24-h incubation, the individual colonies were counted. Three independent experiments were performed with three replicates for each condition.

2.6. Statistical analysis

GraphPad Prism® software version 5.04 (GraphPad Software Inc., La Jolla, CA, USA) was employed to analyse the effects of Cu, using one-way variance analysis (ANOVA) with Tukey post-hoc test. The analyses of differences between Cu-doped compositions and the control 0Cu were performed. Values of $p < 0.05$ were considered statistically significant. For the proteomic evaluations, statistical differences were calculated using the Student's *t*-test, employing the Perseus software. Proteins were considered differentially adsorbed when the ratio of abundance for the two conditions was larger than 1.5 in either direction, and the difference had to be statistically significant ($p \leq 0.05$).

3. Results

3.1. Physicochemical characterisation

Figure 1 displays the SEM images of the developed coatings. The micrographs show the differences between the SAE-Ti surface and the surfaces coated using the sol-gel treatments. The sol-gel material covered the entire area of the metallic substrate although the distribution of the material was heterogeneous; the coating accumulated more in the concavities of the Ti surface formed by the SAE

treatment. No differences were found between the $CuCl_2$-containing coatings and the control (0Cu). The EDX analysis (**Figure 1d'-f'**) detected the elements Ti, Al and O associated with the substrate. Al was found as the result of sandblasting (Al_2O_3 particles) of Ti surfaces. The elements associated with the sol-gel coatings, such as Si and O, and C (related to the organic load of the precursors) were also detected. 0Cu, 0.1Cu and 0.5Cu coatings displayed similar EDX spectra. The Cu and Cl elements were detected only in 1Cu and 3Cu coatings. **Figure 2d** shows the roughness results obtained by optical profilometry. Consistently with the SEM micrographs, there were no statistically significant differences between Ra values for the 0Cu and the Cu-doped coatings.

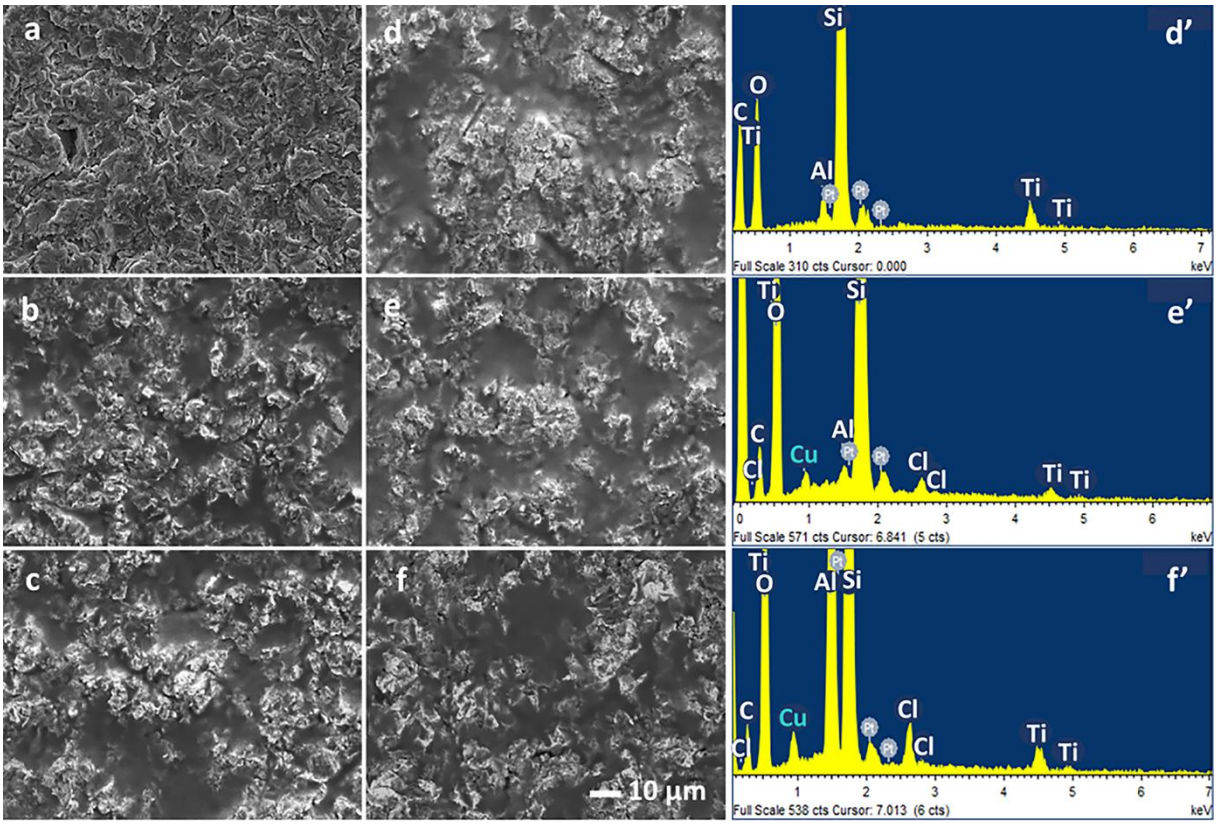

Figure 1. SEM micrographs of SAE-Ti (a), 0Cu (b), 0.1Cu (c), 0.5Cu (d), 1Cu (e) and 3Cu (f). Scale bar, 10 µm. EDX results for 0.5Cu (d'), 1Cu (e') and 3Cu (f').

The XRD patterns for the synthetised sol-gel networks are displayed in **Figure 2a**. As expected, the samples exhibited the typical diffraction spectra associated with amorphous silica with a broad band at 21° (2θ) representing amorphous SiO_2 structures. The signal around 10° (2θ) can be related to the presence of incompletely hydrolysed precursors [23]. The 0.1Cu, 0.5Cu and 0Cu coatings all showed similar XRD patterns, indicating that the addition of $CuCl_2$ did not cause the formation of detectable crystal structures. However, diffraction peaks at 16.5, 22.0 and 34.1° (2θ) assigned to (020), (021) and (002) planes of $Cu(OH)_2$ [24], were found for 1Cu and 3Cu, confirming the presence of Cu^{2+} in these networks. **Figure 2b** shows the FT-IR spectra. The infrared bands at 560, 880 and 1070 cm^{-1}, present

in all the spectra, indicate the silicate network formation [14]. An additional peak at 960 cm^{-1} can be related to Si-OH species [25]. The bands at 1265 and 2970 cm^{-1}, associated with the MTMOS methyl groups, correspond to the Si–C and C–H stretching, respectively [26]. Moreover, the bands around 3350 cm^{-1} and 1600 cm^{-1}, due to –OH stretching [25], change shape and intensity as a consequence of the $CuCl_2$ addition, likely due to the formation of Cu-OH links (as observed using XRD). **Figure 2c** shows the ^{29}Si-NMR results. No changes in the sol-gel network crosslinking were detected after the incorporation of $CuCl_2$. The signals detected between -50 and -75 ppm correspond to the MTMOS precursor (T units), while the signals between -90 and -115 ppm are assigned to TEOS (Q units). Chemical shifts at -58 and -66 ppm can be attributed to T^2 and T^3 species, and signals at -95, -103 and -112 ppm are related to Q^2, Q^3 and Q^4 structures, respectively [14]. The increased intensity of T^3, Q^3 and Q^4 signals showed an elevated crosslinking degree, independent of Cu-doping.

The hydrolytic degradation (mass loss) is shown in **Figure 2e**. The degradation of 0Cu coating continued throughout the experiment, resulting in 40% mass loss after 56 days of incubation in water. The addition of $CuCl_2$ to the sol-gel networks increased the mass loss in comparison with the 0Cu, reaching 68% of initial mass for 3Cu after 56 days of testing. The release kinetics curves (**Figure 2f**) show that the Cu^{2+} ions are liberated very fast during the first 10 h and then the release continues but in a very limited way. The more $CuCl_2$ was added to the coating, the greater was the detected release of Cu^{2+}, reaching the maximum values of 0.1, 0.3, 6.8 and 41.8 ppm for 0.1Cu, 0.5Cu, 1Cu and 3Cu, respectively (after 28 days).

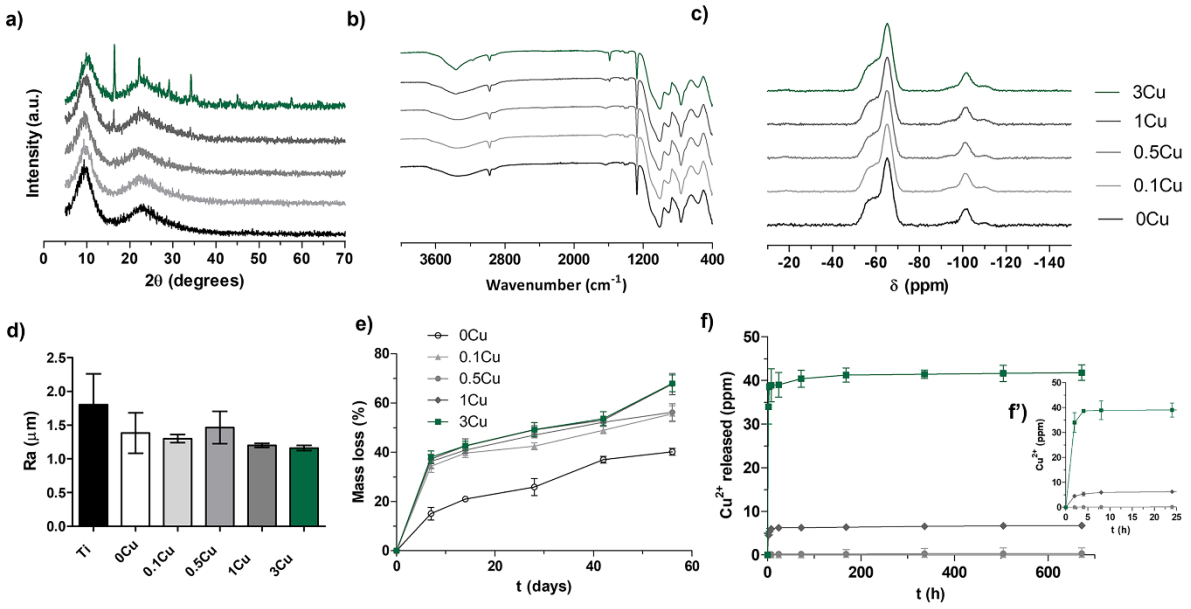

Figure 2. XRD (a), FT-IR (b) and ^{29}Si-NMR (c) patterns for 0Cu, 0.1Cu, 0.5Cu, 1Cu and 3Cu coatings. Arithmetic average of roughness results (d; Ra). Hydrolytic degradation (e) and Cu^{2+} release kinetics (f) for the Cu-doped coatings. (f') Acceleration in the Cu^{2+} release kinetics during the first 25 h of the assay. Bars indicate standard errors.

3.2. *In vitro* assays

3.2.1. Cytotoxicity, cell proliferation and mineralisation

The biomaterials were not cytotoxic towards the HOb cells (data not shown). The effect of Cu-doping on cell proliferation is displayed in **Figure 3a**. The only significant decrease in proliferation was observed for 3Cu coating after 1 day of culture. The addition of Cu to the coatings did not affect the ALP activity after 7 days of incubation (**Figure 3b**). However, a decrease in ALP activity was observed for compositions 0.5Cu, 1Cu and 3Cu after 14 days of culture. The mineralisation capability was assessed using Alizarin Red staining (**Figure 3c**); the formation of calcium deposits was not affected by Cu-doping.

3.2.2. Osteogenic gene expression

The expression of osteogenic genes in HOb cells are shown in **Figure 3d-i**. The expression of RUNX2, OSX and COL1 did not change significantly in the cells exposed to Cu-doped coatings. However, the BMP2 gene increased its expression for all Cu-containing coatings in comparison with 0Cu material after 7 days and for 0.5Cu, 1Cu and 3Cu materials after 14 days. The expression of ALP also increased for 1Cu and 3Cu after 7 days and for 0.1Cu, 0.5Cu and 3Cu after 14 days of incubation. The OCN gene was overexpressed in cells exposed to 0.1Cu and 1Cu for 7 days.

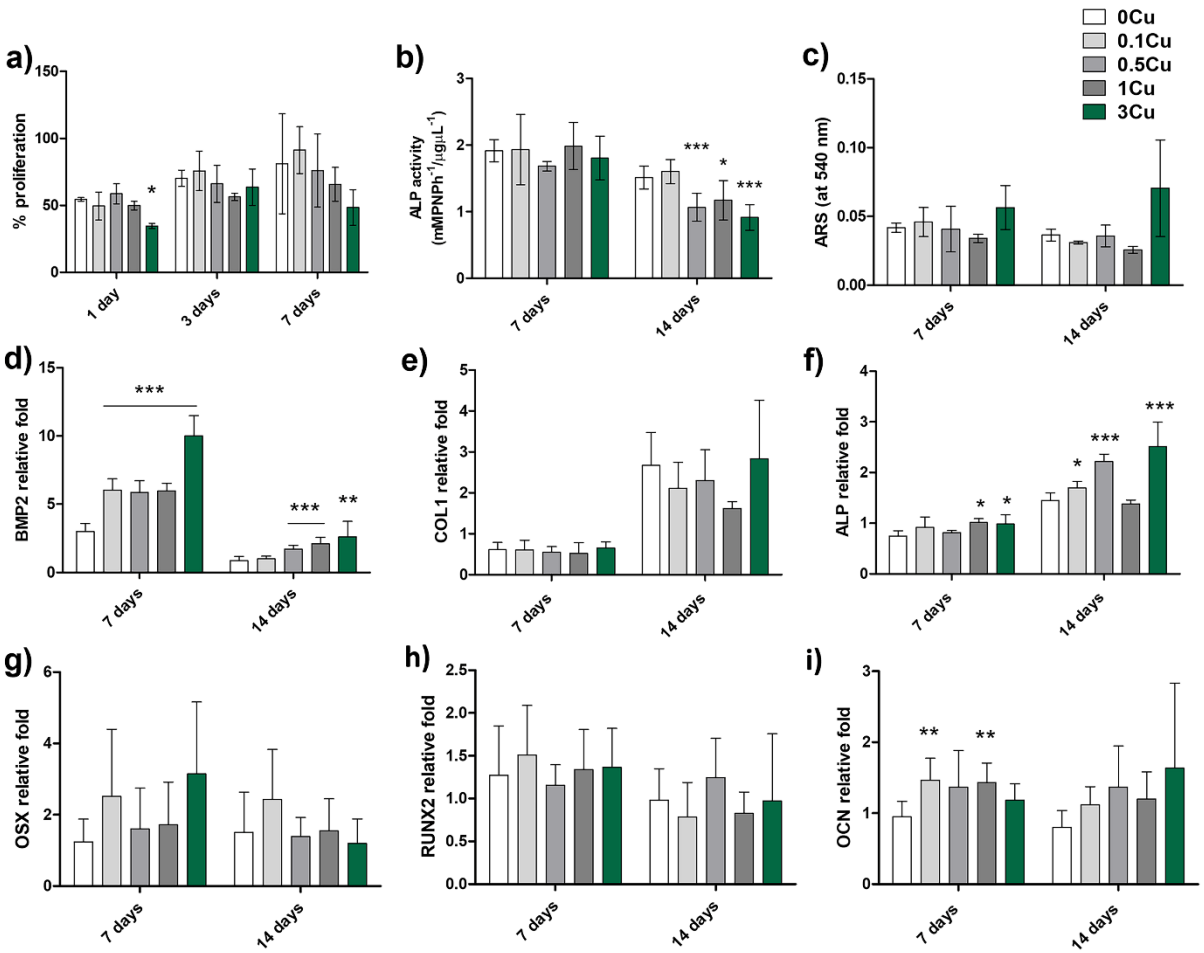

Figure 3. Cell proliferation assay (MTS) after 1, 3 and 7 days (a). The ALP activity (b) and mineralisation capability assessed using ARS (c) at 7 and 14 days. Relative gene expression in HOb cells after 7 and 14 days of culture (d-i). The asterisks ($p \leq 0.05$ (*), $p \leq 0.01$ (**), and $p \leq 0.001$ (***)) indicate statistically significant differences for the Cu-doped coatings in comparison with 0Cu. Results are shown as mean ± SD.

3.2.3. Evaluation of immune response

To evaluate the inflammatory environment induced by Cu, we measured the gene expression and the cytokine liberation by THP-1 cells. **Figure 4a** shows that the expression of pro-inflammatory IL-1β significantly increased in cells exposed to 1Cu for 3 days. Similarly, augmented expression of TNF-α and INFg was detected for the 3Cu material after 3 days of culture (**Figure 4b and c**). The IL-10, related to an anti-inflammatory potential, increased its expression in cells exposed to 1Cu coating at day 1 and for 3Cu coating, after 3 days (**Figure 4d**). The secretion TNF-α and TFG-β cytokines was measured using ELISA (**Figure 4e and f**). A significant increase of pro-inflammatory TNF-α production was found for 3Cu after 1 and 3 days. In contrast, the liberation of anti-inflammatory TFG-β decreased after 1 and 3 days under the same conditions.

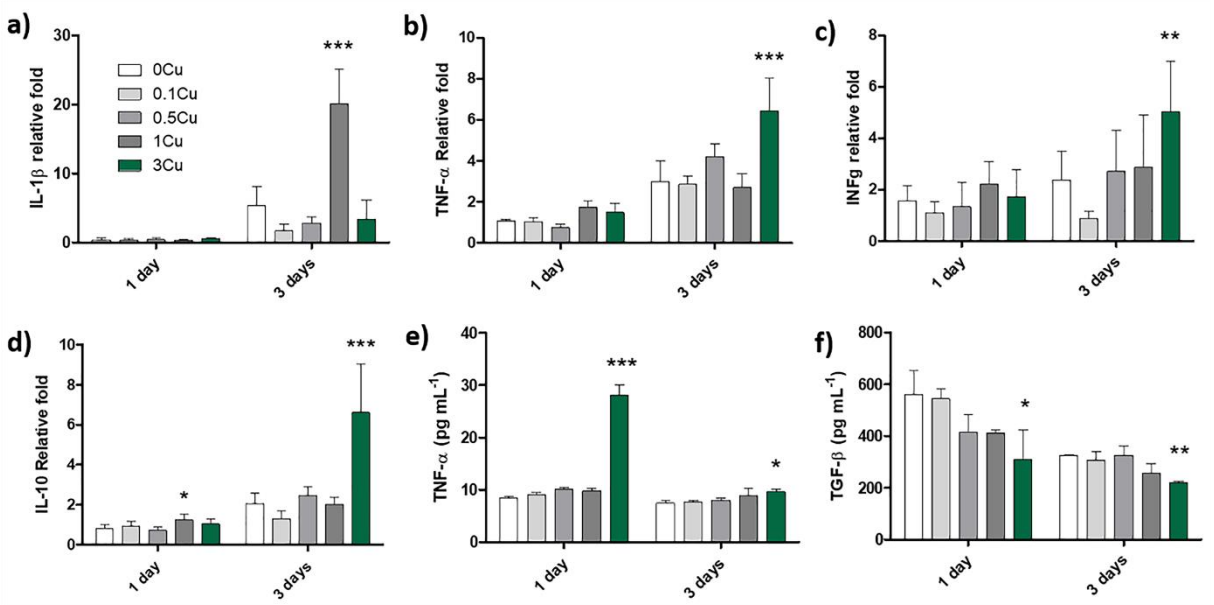

Figure 4. Relative gene expression (a–d) and cytokine liberation (e–f) in THP1 cells after 1 and 3 days of culture. The asterisks ($p \leq 0.05$ (*), $p \leq 0.01$ (**) and $p \leq 0.001$ (***)) indicate statistically significant differences for the Cu-doped coatings in comparison with 0Cu. Results are shown as mean ± SD.

3.3. Antimicrobial activity

The antimicrobial effect of Cu was evaluated against *E. coli* and *S. aureus* by exposing the two bacterial cultures to the Cu-doped coatings for 24 h. The results are shown in **Figure 5**. The growth of blank

control bacteria (incubated in LB medium diluted 50 times) was compared with the growth of the same microorganisms exposed either to the sol-gel composition without Cu (0Cu) or with different concentrations of Cu. The sol-gel coating without Cu (0Cu) had no antibacterial effect when compared to the blank control. In the *E. coli* experiment, the number of colony-forming units (CFUs) was significantly reduced for 0.5Cu in comparison with the blank control. At higher Cu concentrations (1Cu and 3Cu coatings), no growth of *E. coli* was observed. The 1Cu coating showed strong antibacterial activity against *S. aureus*; a complete inhibition of its growth was observed for 3Cu.

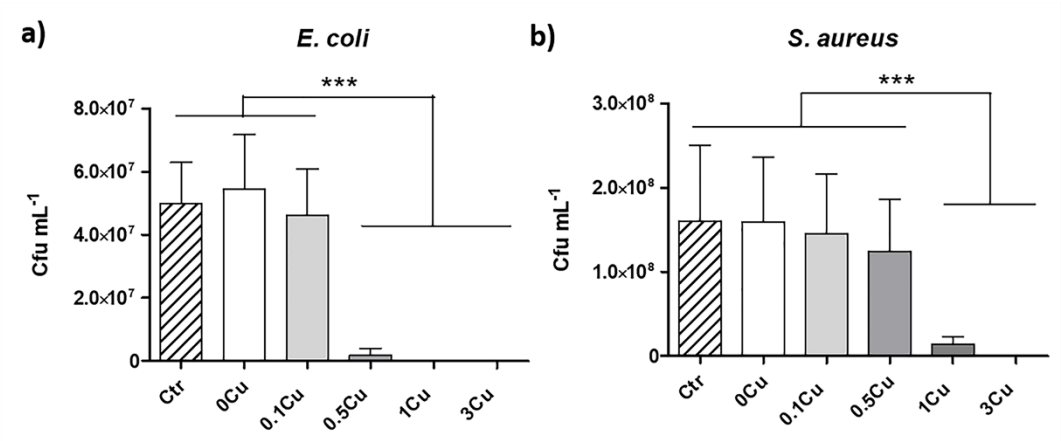

Figure 5. Bacterial growth of a) *E. coli* and b) *S. aureus* after incubation in LB medium alone (Ctr), with the Cu-free coating (0Cu) or with the different Cu-doped coatings. The asterisks ($p \leq 0.001$ (***)) indicate statistically significant differences. Results are shown as mean ± SD.

3.4. Proteomic analysis

To study the effect of Cu on protein binding to biomaterials, coatings with increasing amounts of $CuCl_2$ were incubated with the human serum to form the protein layers. The adsorbed proteins were eluted and analysed using nLC-MS/MS. Two hundred and twenty-one distinct proteins were identified. Comparative analyses were performed for the Cu-enriched samples and the coating without Cu (0Cu). The results revealed that 71 proteins were differentially adsorbed on the coatings due to Cu-doping (**Table S2**). The functions associated with the differentially adsorbed proteins were analysed using bioinformatic resources such as UniProt and DAVID. **Table 1** shows that these proteins are associated with immunity, coagulation, angiogenesis, fibrinolysis and osteogenesis, key functions in bone tissue regeneration.

PANTHER analysis was conducted to classify the proteins differentially more adsorbed onto the Cu-doped surfaces in terms of biological functions and pathways (**Figure 6**). The proteins preferentially attached to 0.1Cu were related to localisation, cellular and multicellular organismal processes, metabolic process and biological regulation biological functions. Adding more Cu to the coatings (0.5Cu, 1Cu and 3 Cu) increased the adsorption of proteins linked to the immune system process, response to

stimulus and interspecies interaction between organisms. Pathway analysis showed that proteins with increased affinity to 0.1Cu and 0.5Cu were associated with the CCKR signalling map. In addition to this pathway, the proteins preferentially adsorbed to 1Cu were associated with blood coagulation. Glycolysis, blood coagulation and plasminogen activating cascade were the pathways detected for the proteins with increased affinity to 3Cu coating.

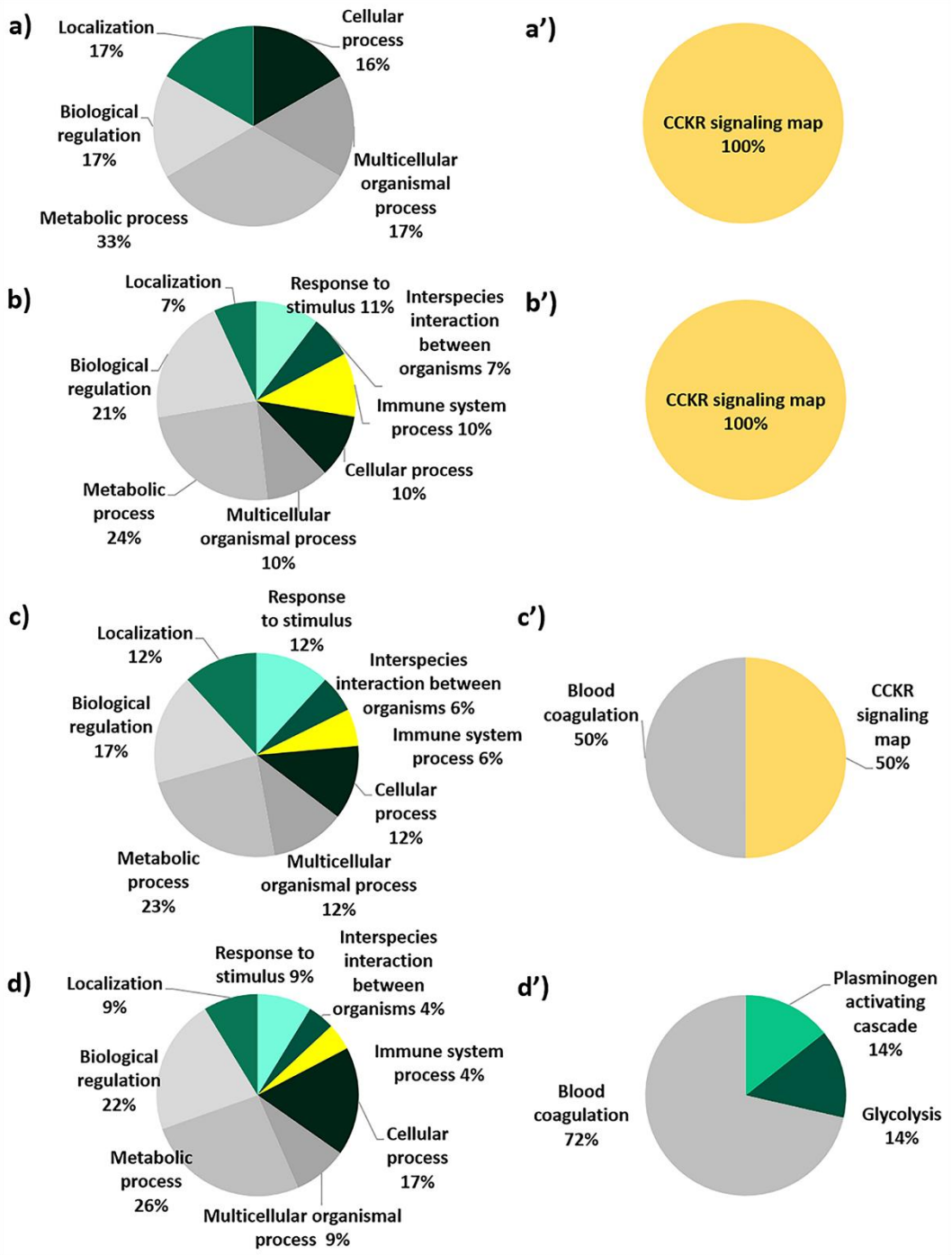

Figure 6. PANTHER pie-charts of biological functions (a-d) and pathways (a'-d') related to the proteins preferentially adsorbed to (a/a') 0.1Cu, (b/b') 0.5Cu, (c/c') 1Cu and (d/d') 3Cu coatings in comparison with 0Cu.

Table 1. Functional analysis of proteins differentially adsorbed (UP/DOWN) onto Cu-enriched coatings in comparison with 0Cu. The proteins were categorised into three functional groups: "immunity", "coagulation, angiogenesis & fibrinolysis" and "osteogenesis".

		0.1Cu/0Cu	0.5Cu/0Cu	1Cu/0Cu	3Cu/0Cu
Immunity	UP	CLUS	C4BPA, SAMP, CO8G, CO4B, C1QA, CLUS, C1QC, CRP, C1S	SAMP, CO8G, CLUS	ENOA, C4BPB, C4BPA, SAMP, CO8B, CO5, FCN3, FCN2
	DOWN	HV118	FCN3, IGHA2, CFAB, A1AG1, A1AG2, LBP, HV103	HVC33, CD14	KV224, KV37, IGLC1, IGHG2, CFAD
Coagulation, angiogenesis & fibrinolysis	UP	-	-	PROS, HRG	PROS, PLMN, FA9, HRG, FA10, HEP2
	DOWN	-	HEP2, ANGT, A2MG, KLKB1, FA12	CXCL7	KLKB1, KNG1, PLF4, FIBA, FA12
Osteogenesis	UP	-	APOE	-	PCOC1
	DOWN	-	-	-	TETN, PEDF, TSK

4. Discussion

Bacterial infections are detrimental to many types of implantations (e.g., peri-implantitis reduces the success rates of dental implants). Compounds with osteogenic and antibacterial properties, such as copper, could help overcome this problem [2]. However, the effects of Cu-doping on biomaterial properties are complex, and the mechanisms are unclear. Using the cell culture approach combined with the analysis of protein adsorption on Cu-doped biomaterials can help widen our knowledge in this field. The present study undertook the first evaluation of the impact of Cu, incorporated at different concentrations in sol-gel coatings, on protein adsorption patterns.

Sol-gel materials with 0.1, 0.5, 1 and 3 wt% $CuCl_2$ were successfully synthesised and applied as coatings onto the SAE-Ti discs. Chemical characterisation showed that the correct sol-gel reactions had taken place, reaching a high degree of crosslinking. The EDX and XRD analyses detected the Cu^{2+} cations only in compositions 1Cu and 3Cu, probably due to the detection limits of these techniques. The diffraction patterns confirmed that Cu was incorporated into the sol-gel network, forming complexes with hydroxyl groups. The introduction of Cu into this network was also reflected by the changes in intensity and shape of the bands associated with these groups in the FT-IR analysis. The addition of Cu increased the rate of hydrolytic degradation of the materials. A controlled Cu^{2+} release was observed; the more $CuCl_2$ was added, the more Cu^{2+} ions were released from the coatings. This was likely due to the greater quantity of the active compound in the network, its increased degradability or both. Here, the greatest amount of Cu^{2+} released, 41.8 ppm, was seen for the composition with 3 wt% $CuCl_2$ after 28 days of

incubation. A critical biological level of 10 ppm Cu^{2+} has been suggested for the survival and growth of 3T3 fibroblasts cultured with a copper-containing glass-based biocomposite [27].

Nevertheless, none of the Cu-enriched sol-gel coatings developed here was cytotoxic towards the HOb cells. Although high levels of Cu^{2+} can compromise the material biocompatibility, the sensitivity of the tested cells to this ion could depend on the type of material from which it is liberated, its release kinetics or even on the cell line evaluated. We observed that incorporating large amounts of $CuCl_2$ (3Cu) impaired cell proliferation after 1 day of culture. However, no differences were found between the levels of proliferation of the cells grown with the Cu-doped and Cu-free coatings for 3 and 7 days. Wu *et al.* [28] have found that Cu-containing mesoporous glass scaffolds do not impair the proliferation of human bone marrow stromal cells (hBMSCs). Moreover, the materials tested in that study showed increased expression of ALP, OPN and OCN genes. However, the ALP activity after 7 days did not significantly differ between the scaffolds with copper and the copper-free controls. In contrast, after 3 days of culture, Cu-bearing stainless steel 317L displayed increased ALP activity and augmented COL1, OPN and RUNX2 gene expression in MC3T3-E1 cells in comparison with Cu-free controls [29]. This effect dissipated over time; after 7 days, no such differences in ALP activity were found, and the gene expression of this marker was lower than in controls. It might be that the Cu-enriched materials accelerate the osteogenic process, with a maximum in ALP activity achieved earlier than in their non-doped equivalents. Here, the Cu-enriched sol-gel coatings did not change the ALP activity, nor did they affect the formation of calcium deposits after 7 days of culture. After 14 days, the ASR analysis did not reveal any significant changes in the mineralisation ability of the cells exposed to Cu-doped materials. However, BMP2, ALP and OCN expression was increased by Cu-doping. These gene expression results suggest that our Cu-enriched sol-gel coatings have an osteogenic effect on HOb cells *in vitro*. This is consistent with the increased BMP2 and OCN gene expression observed in osteoblasts isolated from neonatal rat calvaria, cultured with Cu-ion-substituted hydroxyapatite-based coatings [8].

The effect of Cu-doping on protein adsorption was analysed using proteomic methods. Seventy-one distinct proteins were identified as differentially adsorbed onto the coatings with copper. These proteins were linked to immunity, coagulation, angiogenesis, fibrinolysis and osteogenesis functions. The addition of 0.1 wt% $CuCl_2$ to the coating did not cause significant changes in the protein layer formation. The proteins affected by such small amounts of copper are mainly associated with the immune system, with an increase in the amounts of CLUS (a protein involved in the regulation of the complement system [30]) and a reduction in immunoglobulin HV118 levels. Adding larger amounts of copper resulted in greater changes in the protein adsorption profiles, notably affecting the affinity to proteins related to the immune system response. The complement system is the first line of defence against invading pathogens. Some of the proteins involved in activating this response (C1S, C1QA, C1QC, CO4B and CO8G) and the regulators of this cascade (CLUS and C4BPA) [30,31] were preferentially

adsorbed onto the 0.5Cu coating. Moreover, the CRP and SAMP proteins of the pentraxin superfamily also increased their adsorption as a consequence of Cu-doping. The interaction of pentraxins with the complement system plays an important role in activating and regulating its activity. These proteins are essential for immunosurveillance, antimicrobial immune response and immune homeostasis [32]. In contrast, the FCN3 and CFAB proteins (related to the activation of the complement system via the alternative pathway [31]), HV103 and IGHA2 immunoglobulins and A1AG1, A1AG2 and LBP proteins were found in smaller amounts on 0.5Cu than on undoped coating. Mestriner *et al.* [33] have found that A1AG inhibits neutrophil migration to the site of infection via the nitric oxide-dependent process, resulting in inadequate pathogen clearance. Consequently, the reduced affinity of A1AG1 and A1AG2 to the biomaterials could increase the antibacterial effect. Incorporating 1 wt% of $CuCl_2$ weakened the affinity to CD14 and immunoglobulin HVC33. However, SAMP, CO8B and CLUS increased their adsorption levels. The coating with the highest amount of Cu (3Cu) reduced the adsorption of immunoglobulins (KV224, KV37, IGLC1 and IGHG2) and CFAD protein (related to the complement activation through the alternative pathway [31]). In contrast, the proteins activating the complement system via classical and lectin pathways (FCN3, FCN2, CO5, CO8B), those involved in its regulation (C4BPB, C4BPA) [31] and the pentraxins SAMP and ENOA were preferentially adsorbed onto 3Cu. The ENOA protein showed the highest affinity for 3Cu (15-fold increase in comparison with undoped coating). ENOA can induce early production of pro-inflammatory cytokines, with delayed IL10 production. It takes part in activating the innate immune system, involving a dual mechanism (first, pro-inflammatory and second, anti-inflammatory) [34]. A study by Nguyen *et al.* [35] has reported the potential of ENOA in fighting *Streptococcus dysgalactiae* infections.

Distinct coagulation-related protein signatures depended on the amount of Cu incorporated into the coating. An increased affinity for these proteins was observed for 1Cu and 3Cu materials; larger amounts of PROS and HRG proteins were adsorbed on these coatings than on other materials. PROS not only plays a key role in the regulation of coagulation but also regulates vasculogenesis and angiogenesis [36]. Similarly, the HRG can modulate M1 macrophage polarisation and regulate angiogenesis, fibrinolysis, and coagulation processes [37]. Antibacterial properties of this protein have been also reported against Gram-positive and Gram-negative strains by inducing pathogen lysis [38]. Besides these two proteins, increased adsorption of HEP2, pro-coagulation factors FA9 and FA10 [39] and PLMN (known for its essential role in fibrinolysis [40]) was observed on the 3Cu coating.

A relationship between the level of Cu-doping and the functional characteristics of the proteins adsorbed on the coatings was corroborated by PANTHER results. The presence of copper affected, in a dose-dependent manner, the adhesion of proteins with functions in the coagulation, plasminogen activation and CCKR signalling map pathway (linked to angiogenesis). Moreover, increased adsorption of proteins associated with immune system processes was observed for coatings with $CuCl_2$ levels of

0.5 wt% and higher. This strengthened affinity of Cu-enriched coatings to proteins with immune functions is compatible with their increased immune/inflammatory activity displayed *in vitro* [41]. Here, the materials with the highest Cu content stimulated the expression of IL10 (a marker related to the M2 phenotype polarisation) in THP-1 cells. However, IL-1β, TNF-α and INFg were also overexpressed for these compositions. The augmented expression of these genes, related to the M1 polarisation, is consistent with the significant increase in TNF-α cytokine secretion and the decrease in TFG-β. The response of macrophages to Cu^{2+} has not been studied in depth. However, Díez-Tercero *et al.* [42] have reported that Cu^{2+} concentrations below 0.64 ppm promote the expression of M2-related genes (IL10 and CD206), whereas Cu^{2+} at 6.4 ppm increases the expression of pro-inflammatory TNF-α and CCR7, indicating a tendency towards the M1 polarisation. The increased expression of M1-related markers in cultures exposed to coatings from 1%wt-$CuCl_2$ (releasing up to 6.8 ppm Cu^{2+}) is consistent with the relationship between the concentration of Cu^{2+} and the effects on macrophages. However, a possible link between the increased immune activity in the presence of copper and the detected osteogenic potential must also be considered. Shi *et al.* [43] have reported the osteo-immunomodulatory properties of Cu-containing mesoporous silica nanospheres, which can induce osteogenesis. In the current study, the different signatures of the two proteins associated with the immune reaction and proteins with osteogenic functions (APOE and PCOC1) may help explain the impact of the Cu-doped coatings on osteoblastic cells apart from the effect of Cu^{2+} itself.

The antibacterial properties of Cu-containing sol-gel coatings were evaluated against two model bacteria, *E. coli* (gram-negative) and *S. aureus* (gram-positive). The results demonstrated that Cu-doping confers a strong ability to prevent bacterial infection by either gram-positive or gram-negative strains, consistent with the antibacterial potential attributed to copper [2]. A significant reduction in the growth of *E. coli* was observed for coatings containing 0.5% of Cu or more, whereas for *S. aureus*, this effect was not apparent until 1% of Cu. Complete inhibition of *E. coli* and *S. aureus* growth was reached with the 3Cu coating without any signs of material cytotoxicity. The precise mechanism of antimicrobial activity of Cu-enriched biomaterials remains unclear; the process probably involves combined effects of different pathways that lead to the bacteria killing.

It seems that the antibacterial potential of Cu-sol-gel coatings is directly linked to the influx of Cu ions released from the coatings into the bacteria. The ions could provoke the disruption of the bacterial membrane, resulting in the loss of cytoplasmic content and alterations in the intracellular biochemical processes, triggering the production of oxygen reactive species (ROS) and inducing the DNA damage, thus leading to cell death [44]. However, the antibacterial potential of these Cu-doped sol-gel materials could rely on another, indirect mechanism of action: the macrophage-mediated bactericidal mode. Cu^{2+} can regulate macrophage activity, as demonstrated in this study, and therefore it can promote the bactericidal functions of macrophages [45]. Stafford *et al.* [46] have reported that Cu^{2+} increases the

bactericidal effect of RAW 264.7 macrophages against *E. coli*. Here, the sol-gel coatings with the highest Cu^{+2} content (1Cu and 3Cu) were directly linked to an increased M1-macrophage phenotype activity. Increasing Cu^{2+} levels in the coatings augmented the adsorption of immune-related proteins (e.g., complement system proteins, ficolins and pentraxines) to these surfaces. This could favour the formation of the membrane-attack complex and increase the M1 macrophage activation observed *in vitro*, contributing to the bacteria-killing through this alternative mechanism (**Figure 7**).

Our study showed that the Cu-sol-gel coatings could be involved on two fronts in the fight against pathogens, via the direct antimicrobial effect and through the activation of the immune system. The development of antibacterial materials combining these two mechanisms could become key to preventing infections, especially considering the growing multidrug resistance of pathogens and its related problems. Moreover, our results endorse the proteomic characterisation as a powerful method in developing antibacterial biomaterials associated with a controlled immune response, capable of activating this double mechanism.

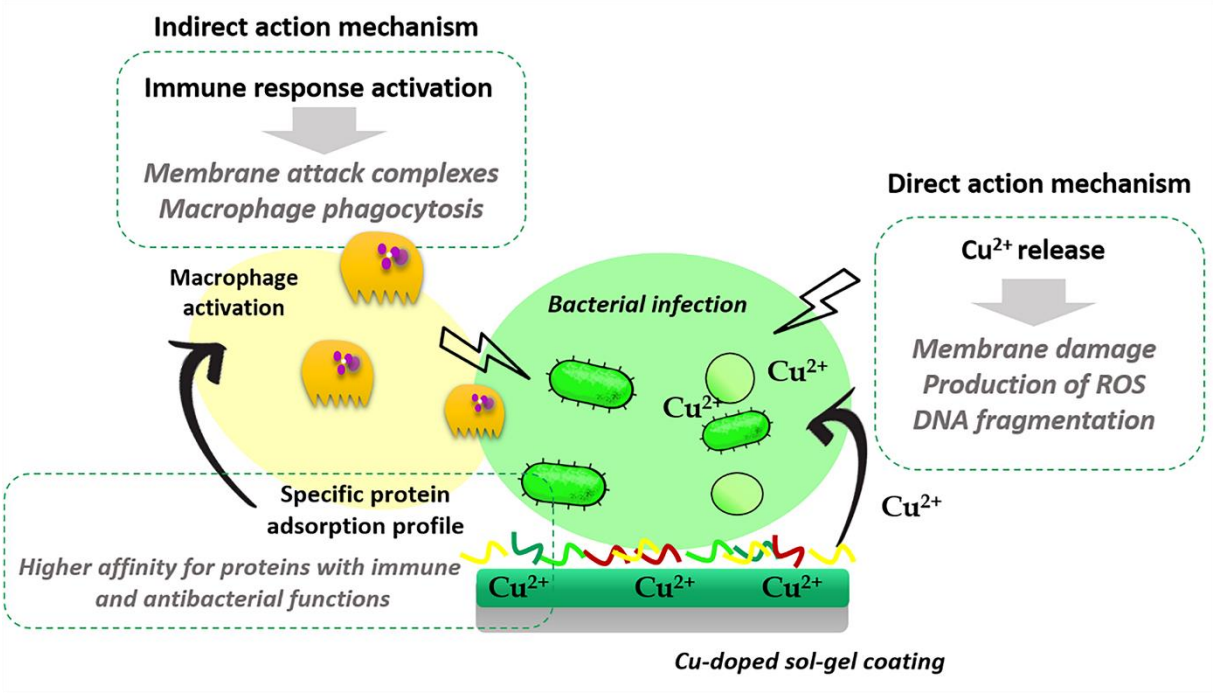

Figure 7. The proposed double mechanism of antibacterial action of the Cu-doped sol-gel coatings.

5. Conclusion

This is the first study addressing the analysis of protein adsorption on biomaterials with antibacterial properties. Sol-gel mixtures with increasing amounts of $CuCl_2$ were successfully synthesised and applied as coatings onto Ti discs. The Cu-doped sol-gel coatings were non-cytotoxic. The tested materials showed osteogenic potential and antibacterial properties against *E. coli* and *S. aureus* bacteria. The increased TNF-α and reduced TGF-β secretion, coupled with the augmented IL-1β, TNF-α and INFg gene expression, indicate that the materials with the highest amounts of Cu (1Cu and 3Cu)

can induce the M1 macrophage phenotype. The Cu ions alter the adsorption of proteins associated with coagulation, angiogenesis, fibrinolysis and osteogenesis functions. They also affect the affinity of the coatings to the proteins involved in the antibacterial effects and the immune response, which is consistent with the macrophage reaction observed *in vitro*. Thus, the changes in the protein adsorption patterns due to Cu-doping, increasing the adsorption of complement system proteins, could favour the membrane-attack complex formation and the macrophage activation, contributing to the defence against pathogens. This effect could indirectly encourage antibacterial behaviour at smaller doses of copper without compromising biocompatibility. Our results contribute to understanding the mechanisms involved in the process of bacteria-killing induced by copper-containing biomaterials.

Acknowledgements

This work was supported by Ministerio Ciencia e Innovación [PID2020-113092RB-C21], Generalitat Valenciana [APOSTD/2020/036, PROMETEO/2020/069], Universitat Jaume I [UJI-B2021-25] and Basque Government [MARSA21/07]. The authors would like to thank Raquel Oliver, José Ortega and Iraide Escobés for their valuable technical assistance and GMI-Ilerimplant for making the titanium discs.

Author Contributions

Francisco Romero-Gavilán: Writing - Original Draft, Data Curation, Investigation, Formal analysis **Iñaki García-Arnáez**: Data Curation, Investigation **Andreia Cerqueira**: Investigation, Writing - Review & Editing **Loredana Scalschi:** Investigation, Writing - Review & Editing **Begonya Vicedo:** Resources, Investigation, Writing - Review & Editing **Alejandro Villagrasa:** Data Curation, Investigation **Raúl Izquierdo:** Resources, Funding acquisition **Mikel Azkargorta:** Data Curation, Investigation **Félix Elortza:** Resources, Investigation **Mariló Gurruchaga:** Writing - Review & Editing, Funding acquisition, Project administration **Isabel Goñi:** Writing - Review & Editing, Funding acquisition, Project administration **Julio Suay:** Writing - Review & Editing, Funding acquisition, Project administration

Conflicts of interest

There are no conflicts to declare.

References

1 I. Cacciotti, *J. Mater. Sci.*, 2017, **52**, 8812–8831.

2 A. Jacobs, G. Renaudin, C. Forestier, J. M. Nedelec and S. Descamps, *Acta Biomater.*, 2020, **117**, 21–39.

3 J. Yang, H. Qin, Y. Chai, P. zhang, Y. Chen, K. Yang, M. Qin, Y. Zhang, H. Xia, L. Ren and B. Yu, *J.*

Orthop. Transl., 2021, **27**, 77–89.

4 G. K. Pouroutzidou, G. S. Theodorou, E. Kontonasaki, I. Tsamesidis, A. Pantaleo, D. Patsiaoura, L. Papadopoulou, J. Rhoades, E. Likotrafiti, C. B. Lioutas, K. Chrissafis and K. M. Paraskevopoulos, *J. Mater. Sci. Mater. Med.*, 2019, **30**, 1–13.

5 S. Moniri Javadhesari, S. Alipour and M. R. Akbarpour, *Colloids Surfaces B Biointerfaces*, 2020, **189**, 110889.

6 I. Burghardt, F. Lüthen, C. Prinz, B. Kreikemeyer, C. Zietz, H. G. Neumann and J. Rychly, *Biomaterials*, 2015, **44**, 36–44.

7 Q. Huang, X. Liu, R. Zhang, X. Yang, C. Lan, Q. Feng and Y. Liu, *Appl. Surf. Sci.*, 2019, **465**, 575–583.

8 Y. Yu, C. Lin, M. Wu and B. Tao, *Mater. Lett.*, 2022, **307**, 131072.

9 S. N. Rath, A. Brandl, D. Hiller, A. Hoppe, U. Gbureck, R. E. Horch, A. R. Boccaccini and U. Kneser, *PLoS One*, 2014, **9**, 1–24.

10 L. B. Romero-Sánchez, M. Marí-Beffa, P. Carrillo, M. Á. Medina and A. Díaz-Cuenca, *Acta Biomater.*, 2018, **68**, 272–285.

11 G. J. Owens, R. K. Singh, F. Foroutan, M. Alqaysi, C. Han, C. Mahapatra and H. Kim, *Prog. Mater. Sci.*, 2016, **77**, 1–79.

12 D. Arcos and M. Vallet-Regí, *Acta Biomater.*, 2010, **6**, 2874–2888.

13 F. Romero-Gavilan, N. Araújo-Gomes, A. M. Sánchez-Pérez, I. García-Arnáez, F. Elortza, M. Azkargorta, J. J. M. de Llano, C. Carda, M. Gurruchaga, J. Suay and I. Goñi, *Colloids Surfaces B Biointerfaces*, 2017, **162**, 316–325.

14 F. Romero-Gavilán, J. Carlos-Almeida, A. Cerqueira, M. Gurruchaga, I. Goñi, I. M. Miranda-Salvado, M. H. Vaz Fernandes and J. Suay, *Prog. Org. Coatings*, 2020, **147**, 105770.

15 M. Martínez-Ibáñez, M. J. Juan-Díaz, I. Lara-Saez, A. Coso, J. Franco, M. Gurruchaga, J. Suay Antón and I. Goñi, *J. Mater. Sci. Mater. Med.*, 2016, **27**, 1–9.

16 K. Wang, C. Zhou, Y. Hong and X. Zhang, *Interface Focus*, 2012, **2**, 259–277.

17 F. Romero-Gavilán, A. M. Sanchez-Pérez, N. Araújo-Gomes, M. Azkargorta, I. Iloro, F. Elortza, M. Gurruchaga, I. Goñi and J. Suay, *Biofouling*, 2017, **33**, 676–689.

18 J. Kim, *Colloids Surfaces B Biointerfaces*, 2020, **188**, 110756.

19 A. Cerqueira, F. Romero-Gavilán, I. García-Arnáez, C. Martinez-Ramos, S. Ozturan, R. Izquierdo, M. Azkargorta, F. Elortza, M. Gurruchaga, J. Suay and I. Goñi, *Mater. Sci. Eng. C*, 2021, **125**, 112114.

20 F. Romero-Gavilán, A. Cerqueira, E. Anitua, R. Tejero, I. García-Arnáez, C. Martinez-Ramos, S. Ozturan, R. Izquierdo, M. Azkargorta, F. Elortza, M. Gurruchaga, I. Goñi and J. Suay, *J. Biol. Inorg. Chem.*, 2021, **26**, 715–726.

21 F. Romero-Gavilán, N. C. Gomes, J. Ródenas, A. Sánchez, F. , Mikel Azkargorta, Ibon Iloro, I. G. A. Elortza, M. Gurruchaga, I. Goñi and and J. Suay, *Biofouling*, 2017, **33**, 98–111.

22 A. Cerqueira, F. Romero-Gavilán, N. Araújo-Gomes, I. García-Arnáez, C. Martinez-Ramos, S. Ozturan, M. Azkargorta, F. Elortza, M. Gurruchaga, J. Suay and I. Goñi, *Mater. Sci. Eng. C*, 2020, **116**, 111262.

23 G. Chernev, N. Rangelova, P. Djambazki, S. Nenkova, I. Salvado, M. Fernandes, A. Wu and L. Kabaivanova, *J. Sol-Gel Sci. Technol.*, 2011, **58**, 619–624.

24 R. Rajakumari, C. Priya and A. Srilekha, *J. Nanosci. Technol.*, 2018, **4**, 435–438.

25 E. Tranquillo, F. Barrino, G. Dal Poggetto and I. Blanco, *Materials (Basel).*, 2019, **12**, 1–12.

26 F. Romero-Gavilán, S. Barros-Silva, J. García-Cañadas, B. Palla, R. Izquierdo, M. Gurruchaga, I. Goñi and J. Suay, *J. Non. Cryst. Solids*, 2016, **453**, 66–73.

27 X. Wang, F. Cheng, J. Liu, J. H. Smått, D. Gepperth, M. Lastusaari, C. Xu and L. Hupa, *Acta Biomater.*, 2016, **46**, 286–298.

28 C. Wu, Y. Zhou, M. Xu, P. Han, L. Chen, J. Chang and Y. Xiao, *Biomaterials*, 2013, **34**, 422–433.

29 L. Ren and K. Yang, *J. Mater. Sci. Technol.*, 2013, **29**, 1005–1010.

30 P. F. Zipfel and C. Skerka, *Nat. Rev. Immunol.*, 2009, **9**, 729–740.

31 N. S. Merle, S. E. Church, V. Fremeaux-Bacchi and L. T. Roumenina, *Front. Immunol.*, 2015, **6**, 1–30.

32 Y. J. Ma and P. Garred, *Front. Immunol.*, 2018, **9**, 1–8.

33 F. L. A. C. Mestriner, F. Spiller, H. J. Laure, F. O. Souto, B. M. Tavares-Murta, J. C. Rosa, A. Basile-Filho, S. H. Ferreira, L. J. Greene and F. Q. Cunha, *Proc. Natl. Acad. Sci. U. S. A.*, 2007, **104**, 19595–19600.

34 C. Guillou, M. Fréret, E. Fondard, C. Derambure, G. Avenel, M. L. Golinski, M. Verdet, O. Boyer, F. Caillot, P. Musette, T. Lequerré and O. Vittecoq, *Sci. Rep.*, 2016, **6**, 1–12.

35 T. T. Thu Nguyen, H. T. Nguyen, Y. T. Wang, P. C. Wang and S. C. Chen, *Fish Shellfish Immunol.*, 2020, **98**, 899–907.

36 L. Suleiman, C. Négrier and H. Boukerche, *Crit. Rev. Oncol. Hematol.*, 2013, **88**, 637–654.

37 Y. Pan, L. Deng, H. Wang, K. He and Q. Xia, *Genes Dis.*, 2020, **9**, 381–392.

38 V. Rydengård, A. K. Olsson, M. Mörgelin and A. Schmidtchen, *FEBS J.*, 2007, **274**, 377–389.

39 H. T. Shiu, B. Goss, C. Lutton, R. Crawford and Y. Xiao, *Tissue Eng. - Part B Rev.*, , DOI:10.1089/ten.teb.2013.0709.

40 C. B. Keragala and R. L. Medcalf, *Blood*, 2021, **137**, 2881–2889.

41 N. Araújo Gomes, F. Romero Gavilán, Y. Zhang, C. Martinez Ramos, F. Elortza, M. Azkargorta, J. J. Martín de Llano, M. Gurruchaga, I. Goñi, J. J. J. P. Van Den Beucken and J. Suay, *Colloids Surfaces B Biointerfaces*, 2019, **181**, 125–133.

42 L. Díez-Tercero, L. M. Delgado, E. Bosch-Rué and R. A. Perez, *Sci. Rep.*, 2021, **11**, 1–13.

43 M. Shi, Z. Chen, S. Farnaghi, T. Friis, X. Mao, Y. Xiao and C. Wu, *Acta Biomater.*, 2016, **30**, 334–344.

44 M. Godoy-Gallardo, U. Eckhard, L. M. Delgado, Y. J. D. de Roo Puente, M. Hoyos-Nogués, F. J. Gil and R. A. Perez, *Bioact. Mater.*, 2021, **6**, 4470–4490.

45 D. Hirayama, T. Iida and H. Nakase, *Int. J. Mol. Sci.*, , DOI:10.3390/ijms19010092.

46 S. L. Stafford, N. J. Bokil, M. E. S. Achard, R. Kapetanovic, M. A. Schembri, A. G. McEwan and M. J. Sweet, *Biosci. Rep.*, , DOI:10.1042/BSR20130014.